LOCAL GRADIENT AND LOCAL MAXIMUM ANALYSIS OF LIDAR DATA FOR TREE CROWN IDENTIFICATION

S. Bruce Blundell, Physical Scientist
U.S. Army Engineer Research and Development Center
Topographic Engineering Center
7701 Telegraph Road
Alexandria, VA 22315-3864
s.bruce.blundell@usace.army.mil

ABSTRACT

Airborne lidar scanning systems are becoming effective tools for tree crown identification and canopy mapping. Canopy height models and their relationship to other forest parameters may be inferred from processed lidar elevation data. This study involved examination of tree canopies depicted by lidar surface models on a tree-by-tree basis, in order to geolocate individual stems and estimate crown extent and density without incorporating a reliable bare-earth model to initially estimate canopy heights. A multi-step approach used local gradient analysis and pulse differencing techniques to first determine reasonable boundaries and extent of the canopy. This overlay served as a template for application of a local maximum algorithm to calculate the image location of a singular apex for each crown. Finally, these apex locations were processed by a crown edge-finding algorithm that averaged results from multiple azimuths to adjust crown centers while estimating their diameters. Results show that small-footprint lidar data on a regular grid with a nominal post spacing of one meter may contain enough information for rapid mapping of individual trees and crown parameters in a discontinuous forest canopy.

Key Words: (1) Lidar, (2) Canopy, (3) Local Gradient, (4) Local Maximum, (5) Crown Apex

INTRODUCTION

The application of laser ranging techniques using both large- and small-footprint lidar systems has become increasingly relevant to forestry applications (Dubayah and Drake, 2000; Andersen, et al., 2006). The use of airborne lidar scanning systems allows the extraction of tree heights for canopy height models and other elements of forest structure (Popescu and Wynne, 2004). If the scanning system is on the ground, accurate measurements of stem diameters may be derived (Watt and Donoghue, 2005). Under certain conditions, analysis of the portion of laser pulse energy that penetrates through the canopy may provide insight into understory characteristics (Maltamo, et al., 2005) and reasonably accurate under-canopy terrain models (Reutebuch, et al., 2003). Lidar remote sensing now plays a role in mapping and modeling forest vegetation from the top of the canopy to the ground surface.

Closely spaced range measurements are provided by rapid laser pulsing from the survey aircraft. Lidar energy is highly reflective and is normally returned from the first surface encountered. Return times are converted to distance from the scanning aircraft platform to any surfaces struck by the pulse energy along the path of the beam. These distances are transformed to geographic elevation and position from the GPS-derived absolute position of the airborne platform. In a forest, the first return should represent the top of the canopy at each pulse location. The last return may represent the ground under the canopy or some intermediate vegetative surface. Significant differences between elevation values for corresponding first and last returns indicate the presence of canopy. Systems with more than two returns may provide details of vertical forest structure.

Lidar systems with a small footprint (on the order of a few centimeters) are common in topographic applications, but may undersample areas of level ground and the tops of tree crowns because the pulses are non-contiguous. Large-footprint, or waveform, lidar systems (pulses 10-25 meters in diameter) emit a greater amount of laser energy and allow the reconstruction of a vertical distribution of vegetation surfaces with finer detail that can be related to above-ground biomass (Drake, et al., 2002). The large footprint also ensures that the apexes of individual tree crowns reflect some of the pulse energy.

Still, high-resolution, small-footprint lidar systems have proven their value in mapping continuous canopy and creating canopy height models. Identification of individual crowns in continuous cover is more challenging. In this work, data from a small-footprint lidar system is used to map a coniferous forest canopy, identify and locate

individual tree crowns, and estimate crown diameters. Given a lidar digital surface model, the forest canopy is mapped by taking advantage of the high-resolution elevation variation of the canopy surface in computing a numerical solution for the directed second derivative, or Laplacian, for each lidar pixel in the data grid. After thresholding these values, a representative digital image overlay is produced over the digital surface model display. A thresholded pulse difference overlay is also created using first and last return data, and is combined with the Laplacian overlay to produce a final canopy overlay. This served as a filter for processing the entire digital surface model with a local surface maximum algorithm in order to identify potential tree crown apexes. Finally, a multi-directional gradient analysis algorithm is applied to each identified crown apex to estimate the crown diameter.

DATASET

The lidar data used in this study was collected in the vicinity of Cooke City, Montana in the southwestern portion of the state, a mountainous area of discontinuous conifer forest. At about 2300 meters above sea level, Cooke City lies in the Soda Butte Creek valley, whose tributaries to the north drain rugged highlands reaching altitudes of 3000 meters. To the south and west lies the high plateau region of Yellowstone National Park.

Lidar data collected in 2003 over this region was provided by the U.S. Army Topographic Engineering Center. The scanning system used was the Optech Airborne Laser Terrain Mapper (ALTM) mounted on a DeHavilland DHC-7 aircraft. Its position was continuously updated during flight with Global Positioning System (GPS) and inertial system data feeds, resulting in absolute positional accuracies of each lidar pulse of ground reflection of approximately 0.5 m in the horizontal and 0.3 m in the vertical. The size of this dataset was 5276 columns by 6601 rows. The final Digital Surface Model (DSM) data, depicting the height of the reflective surface, was provided in 32-bit floating point GeoTIFF format on a regular grid with a one meter sampling interval. The DSM was registered to the WGS-84 ellipsoid.

Several co-registered image products are provided in the ALTM dataset. These include first and last return DSM data, lidar intensity data, a color-coded shaded relief image and a merged intensity and color-coded shaded

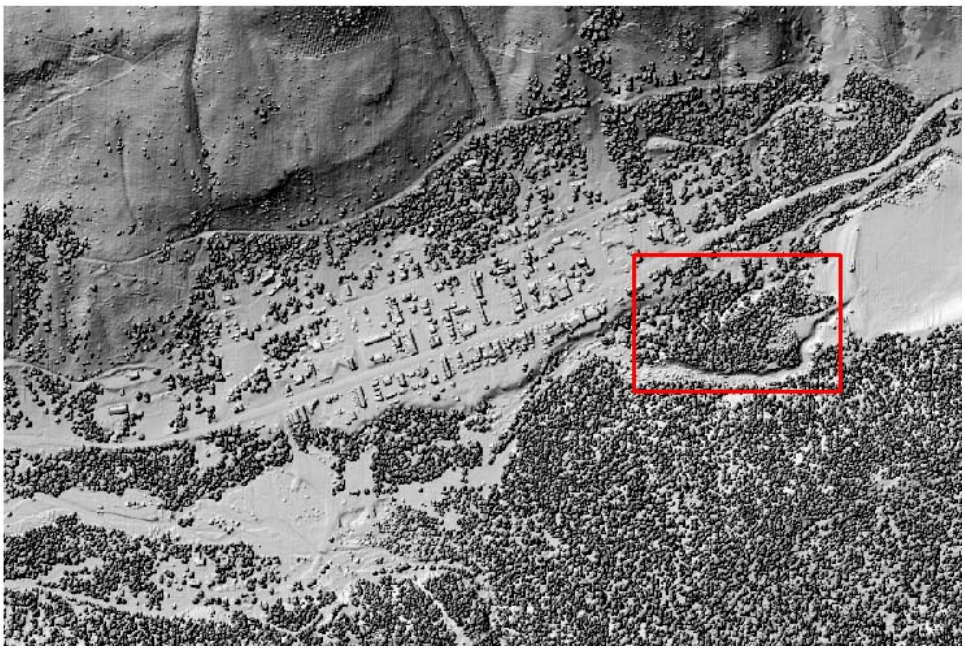

Figure 1. Study Area Lidar First Return Shaded Relief.

relief image. Figure 1 shows the study area, a 1500 x 1000 pixel subset of the Cooke City first return DSM data centered on the town itself, after application of a hillshade algorithm. North is up in the figure, which covers an area of 1.5 by 1.0 kilometers. Aside from town structures, the extent and discontinuous nature of the forest canopy in this

area can be seen by its fine-grained texture in this shaded relief elevation image. The elevations in the study area average about 2350 meters above sea level. At these altitudes, five species dominate the forest cover: subalpine fir, lodgepole pine, whitebark pine, Engelmann spruce, and Douglas fir (DeBlander, 2001). The red box in Figure 1 represents a subset of the study area, 321 x 214 pixels in size, selected for closer analysis and individual crown identification. A shaded relief representation of this subset is depicted in Figure 2, showing variability in the size of individual crowns.

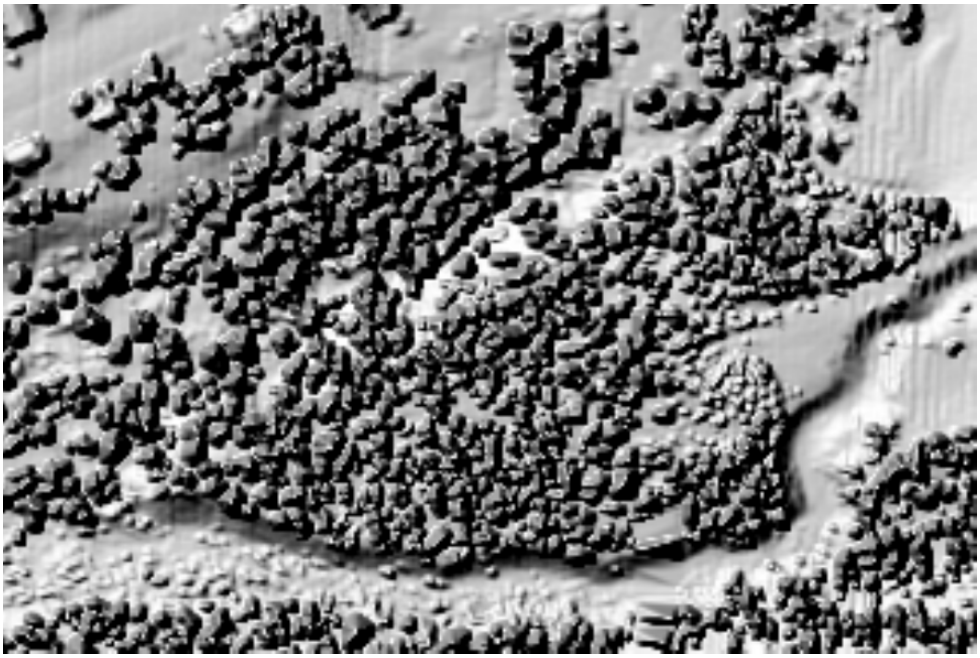

Figure 2. Study Site Subset Shaded Relief.

METHODS

The goal of this work was to take advantage of previous efforts in canopy mapping from small-footprint lidar DSM data in order to detect and map individual tree crowns and estimate their sizes in deriving simple statistics for crown diameter and stem density. Algorithms developed to perform this kind of analysis often depend on a canopy height model (CHM) that provides above-ground crown heights, derived by subtracting the bare-earth or terrain surface from the DSM. The terrain surface may be derived from the last-return lidar pulse data using some form of slope-based algorithm, though it can be difficult to determine which pulses have penetrated the canopy all the way to the ground surface (Cobby, et al., 2001). This may cause underestimation of above-ground canopy heights. The extraction of the terrain surface and estimation of the CHM may be supplemented by ground-based control coordinate elevation and vegetation height measurements (Reutebuch, et al., 2003). Even so, the CHM elevations may be underestimated from another source, the fact that small-footprint lidar pulses often miss treetops and oversample crown shoulders, depending on crown geometry (Nelson, 1997). This can also be a problem with large-footprint, complete-waveform data (Nilsson, 1996). In addition to the undersampling of crown apexes, the resampling of raw lidar pulse data to a regular grid, and the interpolation of gridded first-return values to create a DSM, can add to the underestimation of tree heights (Popescu and Wynne, 2004).

For the general problem of extracting crown apexes from lidar data using a filtering window technique with a local maximum algorithm, choosing the right filter size can avoid errors of commission when the filter size is too small and errors of omission when the filter size is too large. Such errors result in false alarms in the former case and missed truth in the latter. A reliable canopy height model may allow the selection of an appropriate filtering window size when coupled with empirically-derived regression relationships between tree height and crown width (Popescu and Wynne, 2004; Chen, et al., 2006). These relationships are dependent on crown structure. In this work, a CHM is

not employed for filter size estimation. Crown apex false alarms may occur when the filter size is too small for a crown with sub-apex critical points, or false apexes, in its complex structure. Individual trees in this particular dataset, however, have simple crown structures that present a conical canopy form to the lidar scanner. An attempt was made to obviate missed truth errors by using an appropriately small kernel for the ground resolution of this dataset, and comparing its center-weighted mean to the elevation values in a subset of border pixels surrounding the central kernel.

The ENVI image processing and display software environment was used in this work, and all algorithms were developed in ENVI's Interactive Data Language (IDL) programming environment. This allowed rapid testing, thresholding and convenient display of the effect of threshold changes on canopy overlay results. The overall processing scheme from creation of canopy overlays through crown apex extraction and calculation of crown diameters is shown in Figure 3. Each step in this process is discussed below.

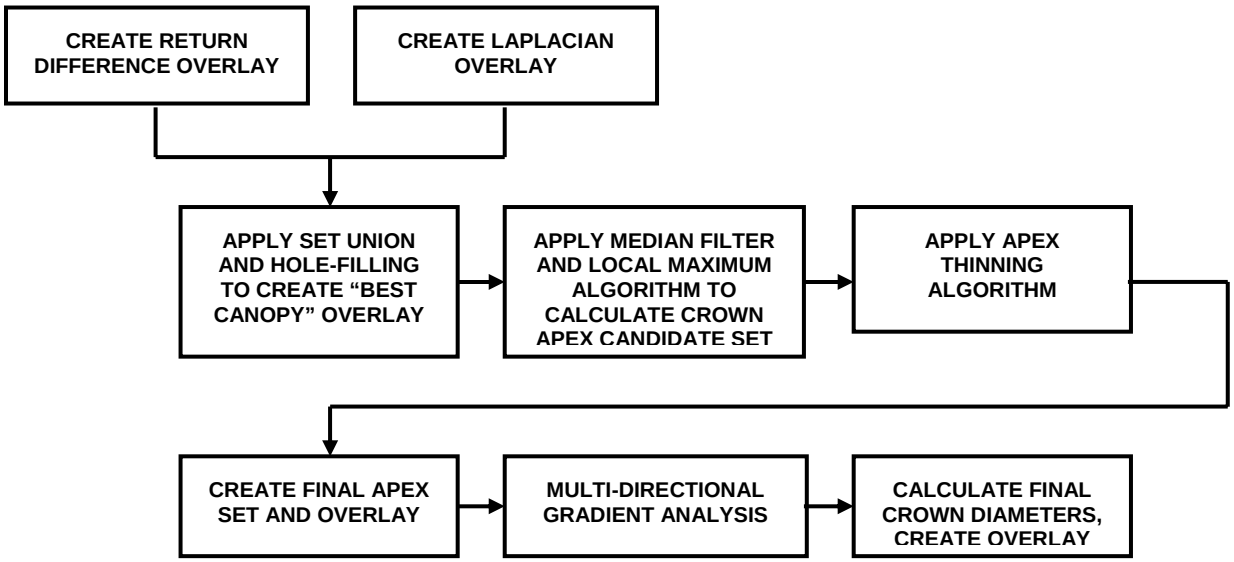

Figure 3. Overall Processing Scheme.

The first part of the process was to generate a canopy overlay co-registered to the lidar DSM within which individual tree locations would be extracted. This was done by combining a pulse-differencing algorithm with a Laplacian-finding technique to create a more complete canopy overlay than that obtained by pulse-differencing methods alone. These methods were used in previous work to create canopy overlays using the same Cooke City dataset described here (Blundell, 2006).

In the pulse-differencing algorithm, elevations from the first-return DSM were subtracted from those of the last return on a pixel-by-pixel basis within the study area. For return differences greater than zero, the overlays created included many obvious non-canopy pixels. After trial-and-error experimentation and examination of a pulse return difference histogram, an optimum lower positive threshold was chosen to exclude very low positive difference pixels that did not spatially correlate with canopy.

Another canopy overlay was then created by mapping small-scale changes in slope in the DSM. In this process, data from only one return is needed. This was done by calculating a numerical solution for the Laplacian of each pixel for a short sequence of DSM elevation values centered on the pixel. Sudden changes in slope were detected using a numerical expression for the second-order, centered finite-divided-difference Taylor series estimation of the Laplacian of the elevation function. This expression, not shown here, solved for the second derivative in a particular direction, and is based on direction-dependent pixel positions as well as the sensor ground sample distance.

Using a 5x5 moving kernel window, a sampling scheme was devised to allow the calculation each pixel's Laplacian values for the progressive set of directions every 45 degrees starting from 0 (straight up or north in the DSM image). For any pixel position in the matrix $S = S(i,j)$ for which the Laplacian $E''_{S,\theta}$ is required in direction θ from position S, elevation values $E_{S+1,\theta}$, $E_{S+2,\theta}$, $E_{S-1,\theta}$, and $E_{S-2,\theta}$ are required in addition to $E_{S,\theta}$ (see Figure 4). In this

way the maximum second derivative and associated direction could be found for each pixel and saved by its matrix position. It was found that these values could then be selectively thresholded to represent canopy pixel locations, and image overlays could be produced depicting canopy extent. The union of the pixel subsets identified by both the Laplacian Taylor series estimation and pulse differencing techniques was then used to create a "best canopy" overlay for further processing. A detailed discussion of the numerical calculations, sampling scheme, developed algorithms, and canopy overlay creation process is provided in a previous work (Blundell, 2006).

After the union of the Laplacian and difference overlays, the "best canopy" overlay still showed occasional untagged pixels in the vicinity of crown centers that might reduce the efficiency of the apex-finding process. These small "holes" were filled in by employing the IDL "MORPH_CLOSE" function that applies a dilation operation followed by a closing operation to a binary image. This has the effect of filling small holes and gaps in the image without affecting primary features. This improved "best canopy" overlay was then used as a template to select DSM pixel elevation values for processing by a local maximum (LM) algorithm. Rather than simply finding the maximum elevation value within the 3x3 LM kernel, the algorithm compared the center-weighted mean of the kernel with the elevation values of a set of pixels bordering the kernel. If the center-weighted mean of the kernel was greater than a specified threshold related to the range of border pixel elevation values, the center pixel of the kernel was tagged as a possible crown apex.

Before application of the LM algorithm, the DSM elevation matrix was subjected to a 3x3 median filter in order to diminish noise in the representation of the canopy surface. While noise is reduced, original elevation values depicting canopy surface complexity and edge information are preserved (Popescu and Kini, 2004).

After applying the median filter and LM process to the study site lidar DSM, it became evident that multiple pixels were often tagged as possible apexes for the same tree crown. A local thinning algorithm was devised to reduce the density of tagged apexes and alleviate this source of errors of commission, given the ground resolution of the dataset. A 3x3 moving kernel was employed to find the mean apex location if more than one candidate apex appeared in the kernel. The mean location was then assigned to the nearest pixel. An overlay was created to display the locations of the final set of tagged apexes over the shaded relief image.

A trial-and-error process was conducted to determine a reasonable kernel center weight factor based on the number of flagged apex pixels. Experiments were performed with two octagonal-shaped border pixel configurations: one based on a 5x5 window enclosing the kernel but with its corners removed, and the other based on a 7x7 enclosing window (Figure 5).

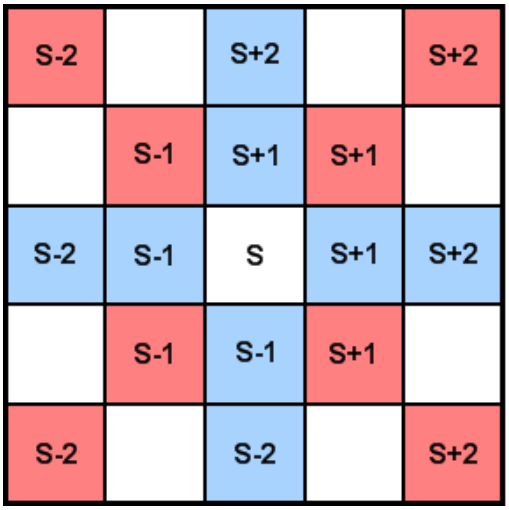

Figure 4. Matrix Positions *S±1* and *S±2* for Laplacian Estimation at Position *S* in Orthogonal (blue) and Diagonal (red) Directions.

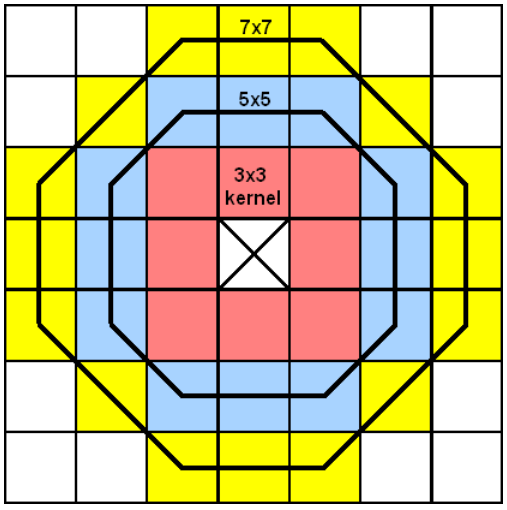

Figure 5. Border Pixel Configurations for Local Surface Maximum Calculations Based on 5x5 and 7x7 Windows.

The final phase of computations involved the estimation of crown diameters for each location in the final set of tagged tree apexes. A multi-directional gradient analysis approach was used, similar to the Laplacian-finding technique for the creation of canopy overlays. The final thinned or final apex overlay was used as a template for

computations centered on each apex for each of eight radial directions in 45 degree increments. For each of the first four radials from 0 to 135 degrees, the Laplacian was calculated for five successive DSM pixels away from the apex, starting from the second pixel for the cases of 0 and 90 degrees. These pixel positions corresponded to distances of 2, 3, 4, 5, and 6 meters. The same process was repeated for each radial in the reverse direction, resulting in 10 Laplacian values along each straight line centered on the apex location, or 40 values in all. The lowest radius value of two meters was limited by the ground sample distance of one meter for this dataset.

For each radial in both forward and reverse directions away from the apex, the maximum Laplacian value was determined and its corresponding radius in meters was saved. Each DSM pixel location was considered to be the center of a 1-meter square cell. For orthogonal directions, the saved radius in meters was simply the pixel distance from the apex to the maximum Laplacian value. For each diagonal direction, the pixel associated with the maximum Laplacian was assigned a radius equal to the integral distance between 2 and 6 that fell within its boundary. This is shown graphically in Figure 6. A column of vertical pixels is identified by their radial distances from the apex. The maximum Laplacian diagonal pixels associated with each integral radius are also identified by the integers 2-6, along with their corresponding orthogonal distances from the center that determine each diagonal pixel's radius assignment. From the figure, it can be seen that the same diagonal pixel is selected to calculate the Laplacian for radius values 5 and 6, since both diagonal radii fall within the pixel's boundary.

Computed crown diameters corresponding to each apex location were then used to create a crown edge overlay in which each crown is represented by an octagonal approximation to a circle whose diameter is given by twice the crown radius saved for the apex in the previous step. These crown edge configurations are shown in Figure 6 in alternating blue and yellow colors. The possible crown diameters are limited to 4, 6, 8, 10 and 12 meters, representing the expected range of diameters encountered for mature trees shown in this dataset. The lower limit is determined by the 3x3 ground resolution of the kernel as depicted in Figure 4. After calculation of the final crown diameter set, crown edge overlays showing octagonal representations of crown extent for each detected apex could then be generated over shaded relief images of the DSM.

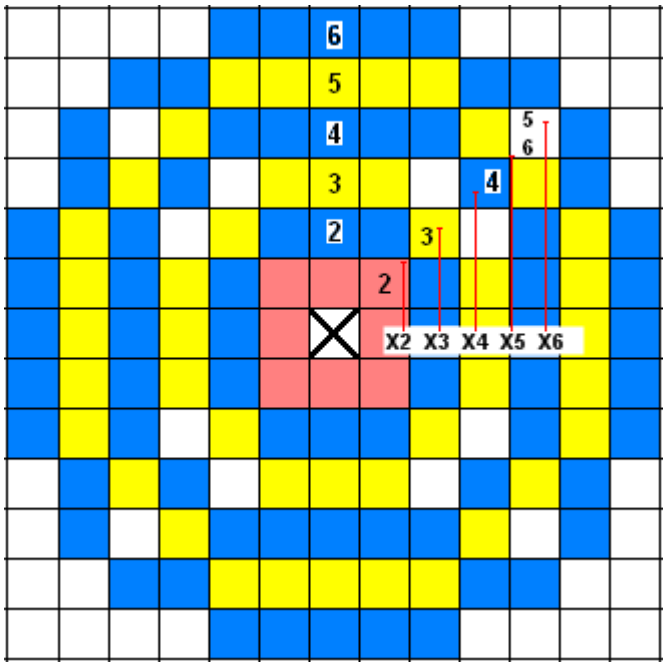

$$X_i = i \sin 45°; i = 2,3,...6$$

$$X_2 = 1.41$$

$$X_3 = 2.12$$

$$X_4 = 2.83$$

$$X_5 = 3.54$$

$$X_6 = 4.24$$

Figure 6. Crown Edge Radii and Pixel Configurations.

RESULTS AND DISCUSSION

In this effort, previous techniques developed for canopy extraction from lidar data served as a basis for algorithm development to identify individual crown apexes and estimate crown diameters for each apex in a coniferous forest. This resulted in a series of overlays displayed over shaded relief images of the lidar DSM showing canopy extent, the final crown apex set, and representative crown edges for a range of diameters.

A lidar return difference overlay was produced by adjustment of a lower difference threshold applied to the difference image to exclude non-canopy pixels, in concert with examination of a histogram of return difference values. First return, last return, and difference image statistics for the study area are provided in Table 1. The return difference histogram is shown in Figure 7, in which a break point is seen separating a central spike containing heavily populated pixel bins and a positive difference 'tail' of bins that extends away from the central spike to the maximum elevation difference. The histogram shows that there were a substantial number of negative difference pixels; these have no physical meaning and appeared randomly distributed throughout the study area when displayed as an overlay (not shown here). For this dataset, it was also evident that the central spike contained spurious non-canopy difference pixels, while the positive tail in the histogram primarily represents the canopy. The break point value of 0.25 meters was therefore used as the lower difference threshold for the overlay. The upper threshold was the maximum elevation difference. Figure 8 shows the final return difference overlay data in red superimposed on the first return shaded relief image of the study area.

Table 1. Study Area Return Elevation Difference Statistics

Image Type	min	max	mean	std. dev.
First return elevation, m	2280.85	2526.02	2346.54	53.11
Last return elevation, m	2280.85	2521.90	2346.09	53.06
Elevation difference, m	-23.43	27.96	0.45	1.91

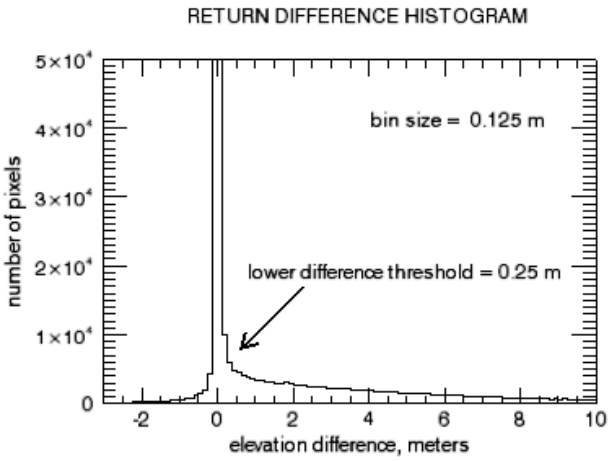

Figure 7. Study Area Difference Image Histogram.

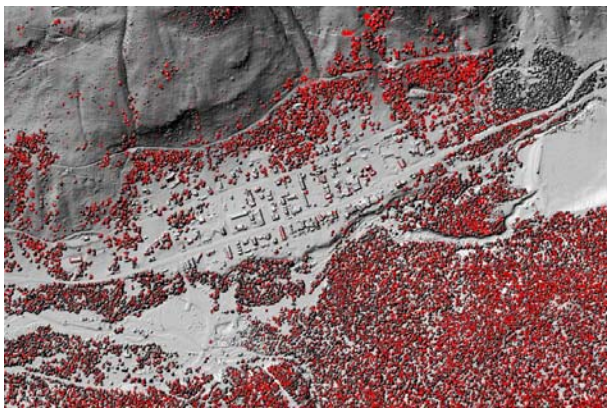

Figure 8. Final Difference Image Overlay.

A Laplacian image was created for the first and last returns and their statistics are provided in Table 2, in which the minimums and maximums are based on absolute values. In this work, only the first return data was used to create the Laplacian overlay used for the "best canopy" overlay. A lower Laplacian threshold for the overlay was chosen in the same manner as for the return difference overlay. The upper threshold used was the maximum Laplacian value. A histogram of Laplacian values for all pixels in the first return DSM is shown in Figure 9. A lower Laplacian threshold of 1.25 was chosen to create a realistic overlay in excluding non-canopy pixels associated with low values clustered around zero.

Table 2. Study Area Laplacian Image Statistics

Image Type	|min|	|max|	mean	std. dev.
First return Laplacian	0	75.44	3.82	5.83
Last return Laplacian	0	72.08	3.74	5.92

A summary of pixel counts for the study area in comparing canopy overlays is provided in Table 3. It is evident that the Laplacian method identifies over four times as many canopy pixels as the pulse differencing method (45.0 to 10.4 percent of study area pixels). The number of canopy pixels tagged by differencing but not by the Laplacian method is very low (0.55 %). The Laplacian method thus captured almost all the canopy pixels identified by differencing. The "best canopy" overlay, after application of the MORPH_CLOSE gap-filling or closing function as described above, contains only 4.4% more of the study area pixels than the final Laplacian overlay (not shown). The "best canopy" overlay is shown in Figure 10. While there appears to be excellent agreement with the canopy areas visible in the study area shaded relief image (Figure 1), there may be some confusion with the edges of structures in the town of Cooke City in the central portion of the area. However, many of these buildings appear to be partially surrounded by trees in the full resolution image. An inspection of the full resolution version of Figure 8 reveals that many of these apparent trees are identified on the final difference overlay.

Table 3. Canopy Overlay Statistics

Parameter	# pixels	% study area
Study area pixels	1500000	100
Pixels above difference threshold	156558	10.44
Pixels above Laplacian threshold	675645	45.04
Pixels above difference and below Laplacian threshold	8270	0.55
Pixels above Laplacian and below difference threshold	508577	33.91
Best canopy after gap-filling closing operation	741117	49.41

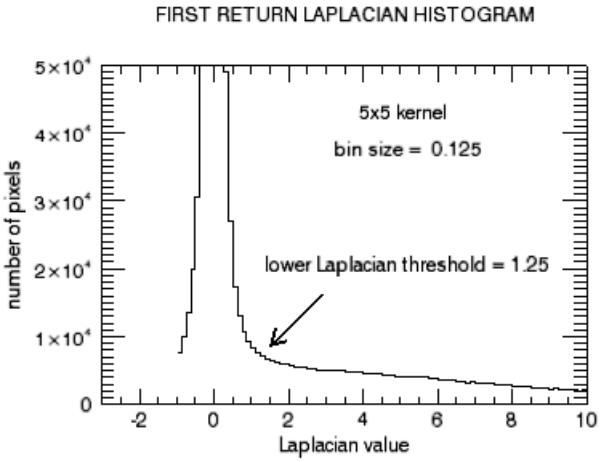

Figure 9. Study Area Laplacian Image Histogram.

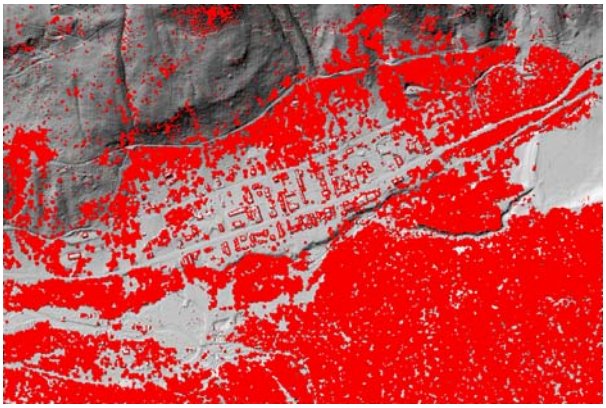

Figure 10. Final Best Canopy Overlay.

The tagged pixels in the "best canopy" overlay were then input into the LM algorithm to calculate candidate apex locations. The effect of border pixel configuration size for the LM algorithm (based on 5x5 and 7x7 windows) was investigated with respect to the set of locations tagged as candidate apexes resulting from comparing the border pixels to the weighted kernel (Figure 5). Table 4 shows candidate and final apex set sizes for both border pixel configurations. The 7x7 window configuration produced a 6% larger initial apex set, but a 15% smaller final set

after thinning. This suggests that the larger configuration produced more clumping of candidate apexes about canopy centers, which are then winnowed by the thinning algorithm.

Experiments were conducted with various center weight values for the 3x3 kernel to determine its effect on the final apex location set after application of the apex thinning algorithm. The sizes of both the initial apex candidate set and the final thinned apex set increased slightly with the center weight value. These figures (not shown) revealed a minimum in the rate of increase at a center weight value of 90, and this figure was used to create the final apex sets.

Table 4. Study Site Apex and Crown Statistics

LM border pixel configuration	Best canopy pixels	Apex candidate set size	Final apex set size	Mean crown dia., m	variance	m^2/crown	Stems/ha.
5x5	741117	132706	15350	6.93	1.27	48.28	207.1
7x7	741117	140708	12997	6.93	1.29	57.02	175.4

The final apex sets were used to create crown edge overlays by multi-directional gradient analysis. Results are given in Table 4, showing consistent mean crown diameters and variances across both LM border pixel configurations. Crown densities represented as m^2/crown and stems/hectare were calculated using the ground area represented by the "best canopy" overlay after the gap-filling function was applied, and not the entire area of the study site. The distribution of calculated integral crown diameters for both LM border pixel configurations is shown in Table 5. Figure 11 is a graphic depiction of the distribution using the 7x7 configuration. Figure 12 shows the crown edge overlay against a black background for better visibility. Due to image compression for publication, the edge configurations do not always appear to be closed features.

Table 5. Study Site Crown Diameter Distributions

LM border pixel configuration	Total crowns	4 meter crown bin	6 meter crown bin	8 meter crown bin	10 meter crown bin	12 meter crown bin
5x5	15350	240	7990	6838	282	0
7x7	12997	233	6708	5813	243	0

In order to qualitatively assess the performance of the apex-finding algorithms and crown diameter calculations on an individual tree basis, the entire processing scheme in Figure 3 was applied to the 321x214 pixel subset shown in Figure 2, using the same canopy overlay and apex calculation parameter choices discussed above for the entire study site. Since the site subset essentially consists of only trees in the above-ground elevation model, potential difficulties with edges of structures tagged by the Laplacian algorithm as canopy are avoided. Final apex and crown statistics for the study site subset are provided in Table 6, while Table 7 provides the site subset crown distributions. These distributions are very similar in form to those for the entire site.

Figure 13 shows the site subset "best canopy" overlay after gap-filling. The overlay pixels have been rendered partially transparent so that the canopy shaded relief model is visible through the overlay. The derived final apex overlay, with each apex location indicated by a small cross on a black background, is provided in Figure 14 for the 7x7 LM border pixel configuration. Figure 15 shows the crown edge overlay in red with calculated crown diameters from the 7x7 distribution given in Table 7.

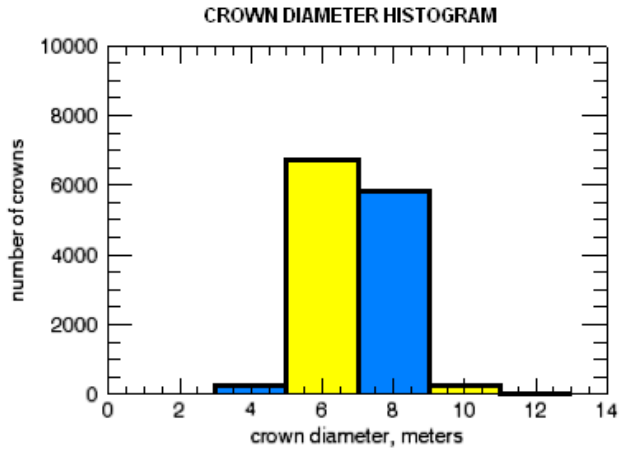

Figure 11. Study Site Crown Diameter Distribution.

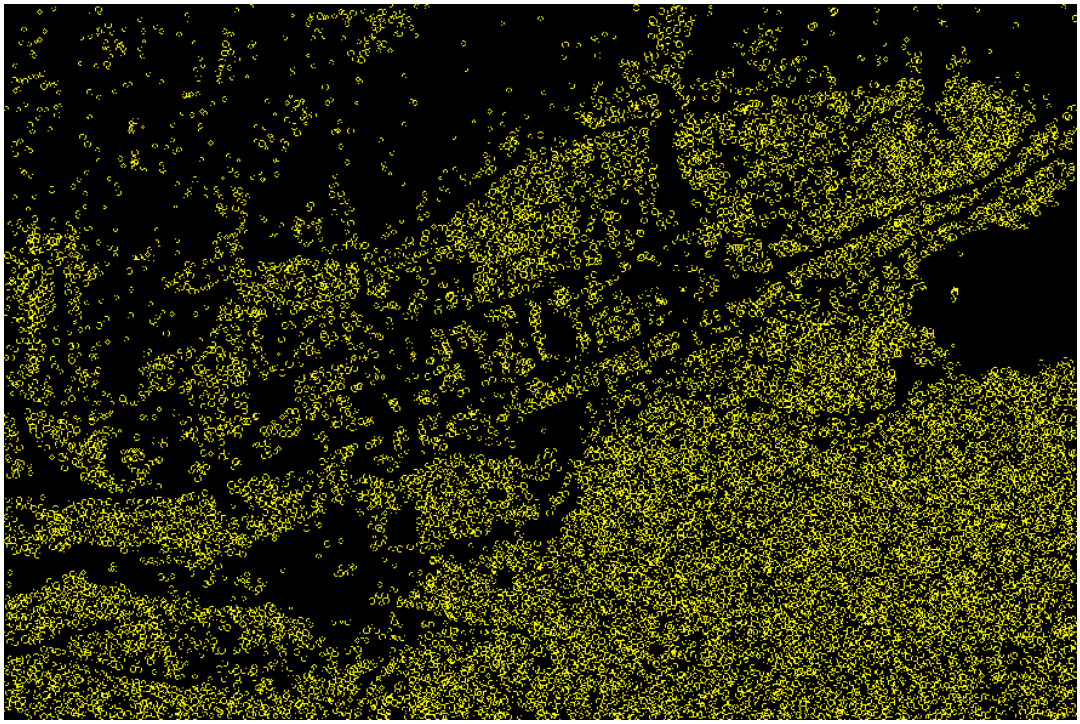

Figure 12. Study Site Crown Edge Overlay.

Table 6. Site Subset Apex and Crown Statistics

LM border pixel configuration	Best canopy pixels	Apex candidate set size	Final apex set size	Mean crown dia., m	variance	m^2/crown	Stems/ha.
5x5	45715	7875	993	7.01	1.28	46.04	217.2
7x7	45151	8146	813	7.04	1.35	55.54	180.1

Table 7. Site Subset Crown Diameter Distributions

LM border pixel configuration	Total crowns	4 meter crown bin	6 meter crown bin	8 meter crown bin	10 meter crown bin	12 meter crown bin
5x5	993	8	504	454	27	0
7x7	813	12	392	385	24	0

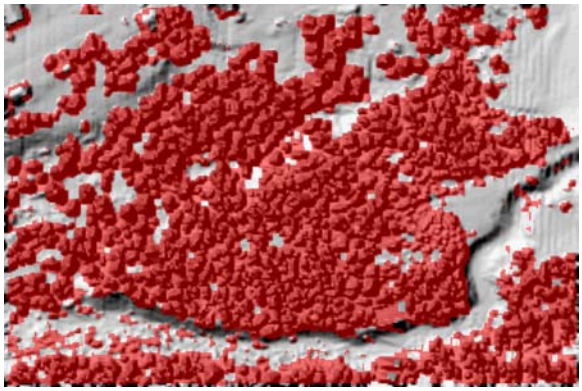

Figure 13. Site Subset "Best Canopy" Overlay.

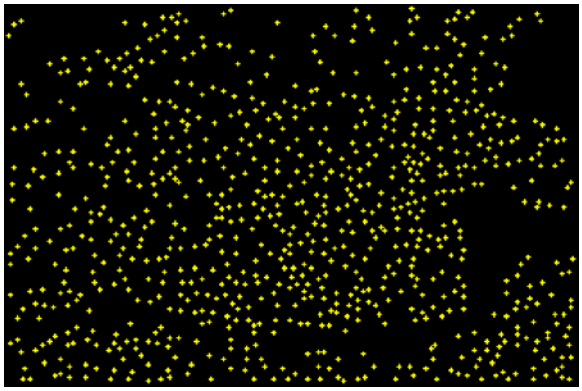

Figure 14. Site Subset Final Apex Overlay.

SUMMARY AND CONCLUSIONS

Along with canopy mapping, small-footprint multiple-return lidar scanners can be effective in estimating the locations of individual trees and some of their structural characteristics. This information is important for models of forest change and structure. This effort was aimed at generating coniferous canopy overlays with pulse differencing and Laplacian-finding techniques, and identifying stem locations and associated crown diameters from these overlays with a combination of a local maximum algorithm and a variation of the Laplacian technique.

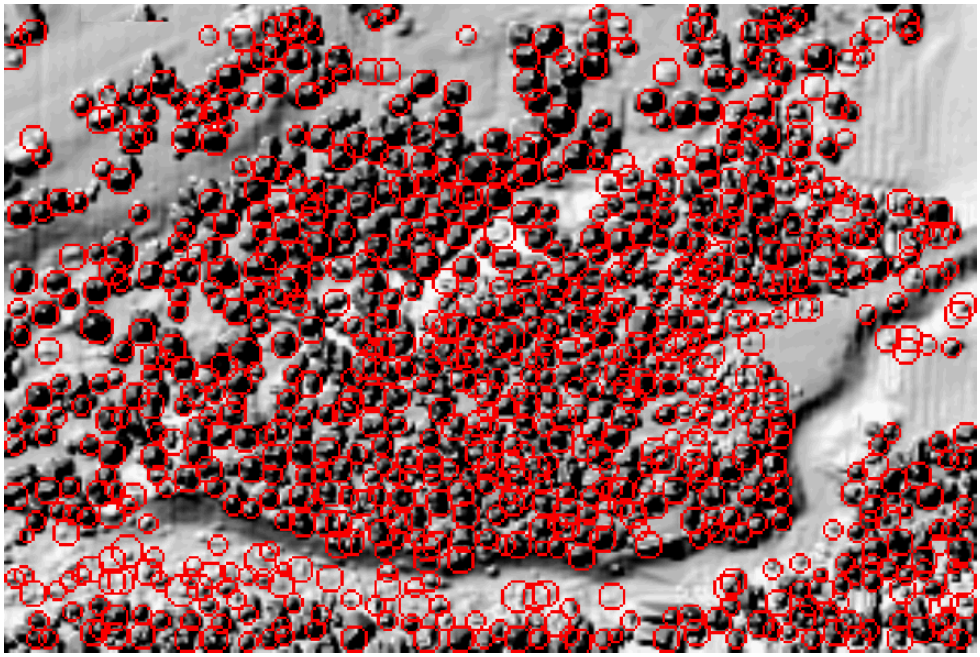

Figure 15. Site Subset Crown Edge Overlay.

While results are encouraging, errors of omission and commission were not estimated with ground survey data. The average number of elevation model cells over each crown was limited by the ground resolution of the dataset. Future work may extend to more complex deciduous canopies allowing realistic attempts at canopy segmentation and error reduction.

These results suggest that for canopies with simple structure, individual crowns may be identified, and their diameters estimated, with lidar elevation models of limited ground resolution without a dependence on canopy height models. An under-canopy terrain elevation model would further allow estimation of additional forest structure parameters.

ACKNOWLEDGEMENTS

The author wishes to thank the U.S. Army Engineer Research and Development Center, Topographic Engineering Center (ERDC-TEC) Imagery Office for providing the lidar data for this effort. Rebecca Ragon (ERDC-TEC) and Melody Clanton (ERDC-TEC) kindly provided graphic support.

REFERENCES

Andersen, H.-E., R.J. McGaughey, and S.E. Reutebuch, 2005. Forest measurement and monitoring using high-resolution airborne lidar, *USDA Forest Service – General Technical Report PNW*, no. 642, pp. 109-120.

Blundell, S.B., 2006. Laplacian analysis and return differencing of lidar data for improved canopy extraction, *Proceedings of the American Society for Photogrammetry and Remote Sensing (ASPRS) Fall Conference, San Antonio, Texas, November 2006.*

Chen, Q., D. Baldocchi, P. Gong, and M. Kelly, 2006. Isolating individual trees in a savanna woodland using small footprint lidar data, *Photogrammetric Engineering and Remote Sensing*, 72(8):923-932.

Cobby, D.M., D.C. Mason, and I.J. Davenport, 2001. Image processing of airborne scanning laser altimetry data for improved river flood modeling, *ISPRS Journal of Photogrammetry and Remote Sensing*, 56:121-138.

DeBlander, L.T., 2001. *Forest Resources of the Gallatin National Forest*, U.S. Department of Agriculture, Forest Service, Rocky Mountain Research Station, June 2001.

Drake, J.B., D.B. Clark, J.B. Blair, R.O. Dubayah, and R.G. Knox, 2002. Sensitivity of large-footprint lidar to canopy structure and biomass in a neotropical forest, *Remote Sensing of Environment*, 81(2-3):378-392.

Dubayah, R.O., and J.B. Drake, 2000. Lidar remote sensing for forestry applications, *Journal of Forestry*, 98(6):44-46.

Maltamo, M., K. Eerikainen, J. Hyyppa, J. Pitkanen, P. Packalen, and X. Yu, 2005. Identifying and quantifying structural characteristics of heterogeneous boreal forests using laser scanning data, *Forest Ecology and Management*, 216(1-3):41-50.

Nelson, R., 1997. Modeling forest canopy heights: The effects of canopy shape, *Remote Sensing of Environment*, 60:327-334.

Nilsson, M., 1996. Estimation of tree heights and stand volume using an airborne lidar system, *Remote Sensing of Environment*, 56:1-7.

Popescu, S.C., and A.U. Kini, 2004. Treevaw: A versatile tool for analyzing forest canopy lidar data – A preview with an eye towards the future, *Proceedings of the American Society for Photogrammetry and Remote Sensing (ASPRS) Fall Conference, Kansas City, Missouri, September 2004.*

Popescu, S.C., and R.H. Wynne, 2004. Seeing the trees in the forest: Using lidar and multispectral data fusion with local filtering and variable window size for estimating tree height, *Photogrammetric Engineering and Remote Sensing*, 70(5):589-604.

Reutebuch, S.E., R.J. McGaughey, H. Andersen, and W.W. Carson, 2003. Accuracy of a high-resolution lidar terrain model under a conifer forest canopy, *Canadian Journal of Remote Sensing*, 29(5):527-535.

Watt, P.J., and D.N.M. Donoghue, 2005. Measuring forest structure with terrestrial laser scanning, *International Journal of Remote Sensing*, 26(7):1437-1446.